

## Charge-carrier mobility in hydrogen-terminated diamond field-effect transistors

Yosuke Sasama,<sup>1,2</sup> Taisuke Kageura,<sup>1</sup> Katsuyoshi Komatsu,<sup>1</sup> Satoshi Moriyama,<sup>1</sup>  
Jun-ichi Inoue,<sup>1</sup> Masataka Imura,<sup>3</sup> Kenji Watanabe,<sup>3</sup> Takashi Taniguchi,<sup>3</sup>  
Takashi Uchihashi,<sup>1</sup> and Yamaguchi Takahide<sup>1,2</sup>

<sup>1</sup>*International Center for Materials Nanoarchitectonics,  
National Institute for Materials Science, Tsukuba 305-0044,  
Japan*

<sup>2</sup>*Graduate School of Pure and Applied Sciences, University of Tsukuba, Tsukuba,  
305-8571, Japan*

<sup>3</sup>*Research Center for Functional Materials, National Institute for Materials Science,  
Tsukuba 305-0044, Japan*

(Dated: 19 May 2020)

Diamond field-effect transistors (FETs) have potential applications in power electronics and high-output high-frequency amplifications. In such applications, high charge-carrier mobility is desirable for a reduced loss and high-speed operation. We recently fabricated diamond FETs with a hexagonal-boron-nitride gate dielectric and observed a high mobility above  $300 \text{ cm}^2\text{V}^{-1}\text{s}^{-1}$ . In this study, we identify the scattering mechanism that limits the mobility of our FETs through theoretical calculations. Our calculations reveal that the dominant carrier scattering is caused by surface charged impurities with a density of  $\approx 1 \times 10^{12} \text{ cm}^{-2}$ , and suggest that an increase in mobility over  $1000 \text{ cm}^2\text{V}^{-1}\text{s}^{-1}$  is possible by reducing these impurities.

## I. INTRODUCTION

Diamond has attracted much attention as a next-generation semiconducting material because of its excellent properties, including a wide-band gap, high thermal conductivity, high breakdown electric field, and high mobility<sup>1</sup>. These properties enable field-effect transistors (FETs) to operate at high temperature with low-energy loss, to resist high voltage, and to be reduced in size. Previously, FETs operating<sup>2</sup> at 400°C and at a breakdown voltage<sup>3</sup> above 2000 V were reported. The diamond FETs in the previous studies were often fabricated using a hydrogen-terminated diamond surface, which exhibits *p*-type surface conductivity.

*p*-type surface conductivity appears on hydrogen-terminated diamond after its exposure to air even if the diamond is non-doped. The surface conductivity can be explained by the transfer doping model<sup>4</sup>. The valence band maximum of hydrogen-terminated diamond is higher than the lowest unoccupied states of impurities adsorbing to the diamond surface due to air exposure. The electrons in the valence bands are therefore transferred to the impurities, and holes are induced at the diamond surface, resulting in surface conductivity. It is known that transfer doping is also caused by exposure to NO<sub>2</sub> gas<sup>5</sup> and by deposition of a solid insulator with a high electron affinity, such as V<sub>2</sub>O<sub>5</sub><sup>6</sup>.

The mobility corresponding to the surface conductivity of hydrogen-terminated diamond is typically 10-100 cm<sup>2</sup>V<sup>-1</sup>s<sup>-1</sup> at room temperature. This value is more than one order of magnitude lower than the intrinsic mobility of bulk diamond ( $\approx 4000$  cm<sup>2</sup>V<sup>-1</sup>s<sup>-1</sup>)<sup>7</sup>. Recently, Li *et al.* calculated the mobility of the surface conductivity of hydrogen-terminated diamond as a function of temperature and carrier density. They pointed out that the major scattering sources were surface impurities<sup>8</sup>.

The mobilities of hydrogen-terminated diamond FETs are almost the same as or less than that of the surface conductivity of hydrogen-terminated diamond. This suggests that charged impurities also exist in the gate insulator. In fact, it was suggested that Al<sub>2</sub>O<sub>3</sub> film deposited by the atomic layer deposition (ALD) method contains oxygen point defects and aluminum vacancies, and electrons trapped in these defects are balanced with hole carriers in diamond<sup>9</sup>. Other gate insulators, such as SiO<sub>2</sub> and CaF<sub>2</sub>, have been formed by vacuum evaporation or sputter deposition, but these films are amorphous and may also contain charged impurities and traps.

Recently, we fabricated diamond FETs using monocrystalline hexagonal boron nitride

(h-BN) as a gate insulator and observed a high mobility above  $300 \text{ cm}^2\text{V}^{-1}\text{s}^{-1}$ .<sup>10</sup> The high mobility is presumably due to the low density of charged impurities in h-BN. In this study, we calculated the room-temperature mobility of diamond FETs as a function of carrier density to reveal the factor limiting the mobility of these FETs.

## II. MODELING

The equations we used for calculating the scattering rate were basically the same as those used in the paper by Li *et al.*<sup>8</sup> There are, however, two major differences between our calculation and theirs. First, Li *et al.* assumed that the density of surface charged impurities was the same as the carrier density. This is reasonable for the surface conductivity of hydrogen-terminated diamond because the negative charges of the surface impurities are balanced with the positive charges of the holes in diamond according to the transfer doping model. In diamond FETs, however, the density of surface charged impurities is independent of the carrier density because the carrier density can be controlled by the gate voltage. We therefore treated the density of the surface charged impurities as a constant. This treatment causes a qualitative difference between the carrier density dependence of the mobility in our calculation and that in the paper of Li *et al.*

The second point of difference is in the way of treating the three valence bands. Li *et al.* used a single equivalent isotropic band model. That is, they assumed a single effective band with a density-of-state mass  $m_d^* = ((m^{\text{LH}})^{3/2} + (m^{\text{HH}})^{3/2} + (m^{\text{SO}})^{3/2})^{2/3}$  and conduction mass  $m_c^* = ((m^{\text{LH}})^{3/2} + (m^{\text{HH}})^{3/2} + (m^{\text{SO}})^{3/2}) / ((m^{\text{LH}})^{1/2} + (m^{\text{HH}})^{1/2} + (m^{\text{SO}})^{1/2})$ . (They used the heavy hole (HH) mass  $m^{\text{HH}} = 0.588m_0$ , light hole (LH) mass  $m^{\text{LH}} = 0.303m_0$ , and split-off (SO) hole mass  $m^{\text{SO}} = 0.394m_0$ , with  $m_0$  being the rest mass.) In contrast, we distinguished the three bands and performed the mobility calculations for the three bands separately. The distribution of the carrier densities in the HH, LH, and SO bands was determined by solving the Schrödinger and Poisson equations self-consistently,<sup>11–13</sup>

$$\left[ -\frac{\hbar^2}{2m_z^i} \frac{d^2}{dz^2} + e\phi(z)(+\Delta^{\text{SO}}) - E_n^i \right] \Psi_n^i(z) = 0, \quad (1)$$

$$\frac{d^2\phi(z)}{dz^2} = -\frac{1}{\epsilon_0\epsilon_s} \left[ eN_{\text{depl}} + e \sum_{i,n} p_n^i |\Psi_n^i(z)|^2 \right], \quad (2)$$

$$p_n^i = \frac{m_{//}^i k_B T}{\pi \hbar^2} \ln \left[ 1 + \exp \left( \frac{E_F - E_n^i}{k_B T} \right) \right], \quad (3)$$

$$\sum_{i,n} p_n^i = p_{2D}. \quad (4)$$

Here,  $e$  is the elementary charge;  $\epsilon_0$  is the vacuum permittivity;  $\epsilon_s$  is the static dielectric constant of diamond;  $e\phi(z)$  is the potential energy;  $N_{\text{depl}} = N_D - N_A$ , where  $N_D$  and  $N_A$  are the ionized donor and acceptor concentrations in the diamond substrate;  $E_n^i$  is the maximum energy of the  $n$ th sub-band;  $\Psi_n^i(z)$  is the wave function corresponding to  $E_n^i$ ;  $p_n^i$  is the sheet hole density of the  $n$ th sub-band;  $p_{2D}$  is the total sheet carrier density;  $E_F$  is the Fermi level;  $k_B$  is the Boltzmann constant; and  $T$  is the absolute temperature. We did not consider the band mixing of the HH, LH, and SO subbands. Examples of  $\Psi_n^i(z)$ ,  $e\phi(z)$ ,  $E_n^i$ , and  $E_F$ , which are the solutions for  $p_{2D} = 1 \times 10^{13} \text{ cm}^{-2}$ , are shown in Fig. 1(a) and 1(b). The carrier densities ( $p^{\text{HH}}$ ,  $p^{\text{LH}}$ , and  $p^{\text{SO}}$ ) for HH, LH, and SO holes were obtained by summing the densities over the seven lowest subbands ( $p^i = \sum_{n=1}^{n_{\text{max}}} p_n^i$ ,  $n_{\text{max}} = 7$ ). The sum of the first HH, LH, and SO subbands reaches  $> 96\%$  of the total carrier density in the range of total carrier density between  $1 \times 10^{11}$  and  $1 \times 10^{14} \text{ cm}^{-2}$  (Fig. 1(c)).  $\Delta^{\text{SO}}$  is the spin-orbit gap energy and is taken into account only in the calculation of the split-off holes.  $\Delta^{\text{SO}}$  of diamond is  $6 \text{ meV}^{14}$ . A secondary ion mass spectrometry measurement on a diamond substrate similar to the ones we used for fabricating the FETs indicated that the concentration of nitrogen, which acts as a donor, is 0.5 ppm and that of boron, which acts as an acceptor, is 5 ppb. Although these values may vary in the substrate and there may be defects (*e.g.* vacancies) that influence the value of  $N_{\text{depl}}$ , we assumed  $N_{\text{depl}} = 0.5 \text{ ppm}$ . We used the following effective masses obtained from the Luttinger parameters<sup>15</sup> for the (111) diamond surface:

$$m_z^{\text{HH}}/m_0 = 1/(\gamma_1 - 2\gamma_3) = 0.763, \quad (5)$$

$$m_z^{\text{LH}}/m_0 = 1/(\gamma_1 + 2\gamma_3) = 0.248, \quad (6)$$

$$m_z^{\text{SO}}/m_0 = 1/\gamma_1 = 0.375, \quad (7)$$

$$m_{//}^{\text{HH}}/m_0 = 1/(\gamma_1 + \gamma_3) = 0.299, \quad (8)$$

$$m_{//}^{\text{LH}}/m_0 = 1/(\gamma_1 - \gamma_3) = 0.503, \quad (9)$$

$$m_{//}^{\text{SO}}/m_0 = 1/\gamma_1 = 0.375, \quad (10)$$

where  $m_z^i$  is the effective mass along the  $z$  direction perpendicular to the diamond surface and  $m_{//}^i$  is the effective mass parallel to the diamond surface.

The above self-consistent calculation was performed for a given hole density  $p_{2D}$ . The gate voltage  $V_{GS}$  corresponding to the hole density is expressed as

$$V_{GS} = -\frac{e(p_{2D} + n_{\text{depl}} - n_{\text{imp}})t_{\text{hBN}}}{\epsilon_{\text{hBN}}} + \psi_s + \phi_{\text{ms}} \quad (11)$$

Here,  $n_{\text{depl}}$  ( $n_{\text{depl}} = N_{\text{depl}}z_{\text{depl}}$ , where  $z_{\text{depl}}$  is the depletion-layer thickness) is the sheet density of the fixed charge in the depletion layer and  $n_{\text{imp}}$  is the sheet density of charged impurities at the diamond surface (see below).  $t_{\text{hBN}}$  and  $\epsilon_{\text{hBN}}$  are the thickness and dielectric constant of the h-BN gate dielectric.  $\psi_s$  ( $<0$ ) is the surface potential (relative to deep inside the diamond).  $\phi_{\text{ms}} = \phi_{\text{m}} - \phi_{\text{s}}$  is the difference between the work function ( $\phi_{\text{m}}$ ) of the metal gate and that ( $\phi_{\text{s}}$ ) of hydrogen-terminated diamond.  $\phi_{\text{s}} \approx 0.3$  eV, because the electron affinity of hydrogen-terminated diamond is  $-1.3$  eV<sup>16</sup> and the Fermi level in the bulk diamond with  $N_D$  (nitrogen) = 0.5 ppm and  $N_A = 5$  ppb is  $-1.6$  eV below the conduction band minimum.  $\phi_{\text{m}}$  for titanium (Au/Ti gate) is  $4.3$  eV<sup>17</sup>. Therefore,  $\phi_{\text{ms}} \approx 4.0$  eV. For the given  $p_{2D}$ ,  $n_{\text{depl}}$  and  $\psi_s$  were evaluated by performing the Schrödinger-Poisson calculation.  $n_{\text{imp}}$  was determined by comparing the experimental and calculated mobilities, as described below. An example of the deduced  $V_{GS} - p_{2D}$  relationship is shown in Fig. 1(d). The  $V_{GS} - p_{2D}$  curve is in good agreement with the experimental one if a slightly different value of  $N_D$  ( $\approx 2$  ppm) is used; there may be such a level of spatial variation in  $N_D$  in an HPHT (high pressure high temperature) IIa diamond substrate.

Next, we calculated the scattering rate for heavy, light, and split-off holes. The calculation took into account four scattering mechanisms: surface impurity scattering, background ionized impurity scattering, acoustic phonon scattering, and surface roughness scattering. Optical phonon scattering was not considered because the optical phonon energy is as large as 165 meV and the occupation number of optical phonons is small at room temperature in diamond<sup>18</sup>.

The scattering rate equations for the four different mechanisms are described below.

#### A. Surface charged impurity scattering

The carriers are scattered by the Coulomb potential arising from charged impurities on the surface. The scattering rate due to charged impurities at a distance  $d$  above the diamond

surface is given by

$$\frac{1}{\tau_{\text{imp}}^i} = n_{\text{imp}} \frac{m_{//}^i}{2\pi\hbar^3(k_F^i)^3} \left( \frac{e^2}{2\epsilon_0\epsilon_s} \right)^2 \int_0^{2k_F^i} [F^i(q)]^2 \frac{\exp(-2qd)}{[q + q_{TF}^i G^i(q)]^2} \frac{q^2 dq}{\sqrt{1 - (q/2k_F^i)^2}}, \quad (12)$$

$$F^i(q) = \int_0^\infty dz |\Psi_1^i(z)|^2 \exp(-qz), \quad (13)$$

$$G^i(q) = \int_0^\infty dz \int_0^\infty dz' [\Psi_1^i(z)]^2 [\Psi_1^i(z')]^2 \exp(-q|z - z'|). \quad (14)$$

Here,  $n_{\text{imp}}$  is the density of surface charged impurities,  $\hbar$  is the reduced Planck constant,  $q_{TF}^i = m_{//}^i e^2 / (2\pi\epsilon_0\epsilon_s\hbar^2)$  is the Thomas-Fermi screening wave vector,  $F^i(q)$  and  $G^i(q)$  are form factors,  $k_F^i = \sqrt{2\pi p^i}$  is the Fermi wave vector, and  $d$  is the distance between carriers and surface charged impurities. In order to calculate the form factors, we used the wave function of the first subband of HH, LH, and SO obtained from the self-consistent calculation of the Schrödinger and Poisson equations. When we used Fang-Howard wave functions with  $b^i = [12me^2(N_{\text{depl}} + 11p^i/32)/(\hbar^2\epsilon_0\epsilon_s)]^{1/3}$ , the results were qualitatively the same. In this case,  $F^i(q) = [b^i/(b^i + q)]^3$ , and  $G^i(q) = 1/8\{2[b^i/(b^i + q)]^3 + 3[b^i/(b^i + q)]^2 + 3[b^i/(b^i + q)]\}$ .

## B. Background ionized impurity scattering

Ionized impurities in the substrate (background ionized impurities) induce carrier scattering. The scattering rate due to background ionized impurities is given by (Ref.<sup>19</sup>)

$$\frac{1}{\tau_{\text{impbulk}}^i} = n_{\text{imp}}^{(3D)} \frac{m_{//}^i}{2\pi\hbar^3(k_F^i)^3} \left( \frac{e^2}{2\epsilon_0\epsilon_s} \right)^2 \int_0^{2k_F^i} \frac{1}{(q + q_{TF}^i)^2} \frac{q dq}{\sqrt{1 - (q/2k_F^i)^2}}. \quad (15)$$

Here,  $n_{\text{imp}}^{(3D)} = N_D + N_A$  is the density of background ionized impurities; the donors and acceptors should be fully ionized near the surface because of band bending.

## C. Acoustic phonon scattering

A phonon is a quantum of lattice vibration and causes carrier scattering. There are two modes of lattice vibration: acoustic and optical. The room-temperature mobility of diamond is mainly affected by acoustic phonons<sup>8</sup>. The scattering rate due to acoustic phonons is given by

$$\frac{1}{\tau_{\text{ac}}^i} = \frac{m_{//}^i k_B T D_{\text{ac}}^2}{\rho u_l^2 \hbar^3} \int_{-\infty}^\infty |\Psi_1^i(z)|^2 |\Psi_1^i(z)|^2 dz. \quad (16)$$

Here,  $D_{\text{ac}}$  is the acoustic deformation potential,  $\rho$  is the crystal mass density, and  $u_l$  is the velocity of longitudinal acoustic phonons. The deformation potential of diamond was

calculated to be 8 eV by Cardona *et al.* using the linear combination of muffin tin orbitals (LMTO) method.<sup>20</sup> This value is consistent with the temperature dependence of the mobility of boron-doped diamond found in the study by Pernot *et al.*<sup>18</sup>.  $\rho$  and  $u_l$  of diamond are  $3515 \text{ kgm}^{-3}$  and  $17536 \text{ ms}^{-1}$ , respectively<sup>18</sup>. For the Fang-Howard wave functions,  $\int_{-\infty}^{\infty} |\Psi_1^i(z)|^2 |\Psi_1^i(z)|^2 dz = 3b^i/16$ .

#### D. Surface roughness scattering

Surface roughness induces disorder in the electric potential and leads to carrier scattering. The scattering rate due to surface roughness is given by

$$\frac{1}{\tau_{\text{sr}}^i} = \frac{\Delta^2 \Lambda^2 e^4 m_{\parallel}^i}{(\epsilon_0 \epsilon_s)^2 \hbar^3} (p_{2\text{D}} + n_{\text{depl}})^2 \int_0^1 \frac{u^4 \exp[-(k_F^i)^2 \Lambda^2 u^2]}{[u + G^i(2k_F^i u) q_{TF}^i / (2k_F^i)]^2 \sqrt{1-u^2}} du. \quad (17)$$

The surface roughness is characterized by the average roughness ( $\Delta$ ) and correlation length ( $\Lambda$ ).

The total scattering rate is calculated using the Mathiessen rule,

$$\frac{1}{\tau^i} = \frac{1}{\tau_{\text{imp}}^i} + \frac{1}{\tau_{\text{impbulk}}^i} + \frac{1}{\tau_{\text{ac}}^i} + \frac{1}{\tau_{\text{sr}}^i}, \quad (18)$$

and the mobility for  $i=\text{HH}$ ,  $\text{LH}$ , and  $\text{SO}$  is obtained from  $\mu^i = e\tau^i/m_{\parallel}^i$ . We calculated the carrier density and mobility of the FET using the formula for the multi-carrier Hall effect, because our experimental results were obtained from low-magnetic-field Hall-effect measurements,

$$\mu = \frac{p^{\text{HH}}(\mu^{\text{HH}})^2 + p^{\text{LH}}(\mu^{\text{LH}})^2 + p^{\text{SO}}(\mu^{\text{SO}})^2}{p^{\text{HH}}\mu^{\text{HH}} + p^{\text{LH}}\mu^{\text{LH}} + p^{\text{SO}}\mu^{\text{SO}}}, \quad (19)$$

$$p = \frac{(p^{\text{HH}}\mu^{\text{HH}} + p^{\text{LH}}\mu^{\text{LH}} + p^{\text{SO}}\mu^{\text{SO}})^2}{p^{\text{HH}}(\mu^{\text{HH}})^2 + p^{\text{LH}}(\mu^{\text{LH}})^2 + p^{\text{SO}}(\mu^{\text{SO}})^2}. \quad (20)$$

### III. RESULTS AND DISCUSSION

Figure 2 shows the carrier density dependence of mobility of our three diamond FETs with h-BN gate dielectric<sup>10</sup>. The figure also shows the mobilities of diamond FETs reported by other groups and the mobility of surface conductivity of hydrogen-terminated diamond surfaces exposed to air<sup>10</sup>. The mobilities of our FETs exceeded  $300 \text{ cm}^2\text{V}^{-1}\text{s}^{-1}$ , and they were only weakly dependent on the carrier density. This contrasts with the mobilities of the

surface conductivity induced by air exposure, which decreases monotonically with carrier density.

Here, let us identify which scattering mechanism limits the mobility of our FETs. The carrier density dependence of the mobility limited by acoustic phonon scattering is basically determined by material-dependent parameters such as the deformation potential and phonon velocity. As shown in Fig. 2, the calculated acoustic-phonon-limited mobility is more than one order of magnitude higher than the experimental one, and therefore, acoustic phonons are not the dominant scattering sources in our FETs. The high acoustic-phonon-limited mobility is due to the high phonon velocity and the large crystal mass density in diamond.

The analytical formula for the surface roughness scattering contains device-dependent parameters,  $\Delta$  and  $\Lambda$ , which characterize the magnitude of surface roughness. Here, we will assume  $\Delta = 0.3$  nm and  $\Lambda = 2$  nm. The validity of these values is described below. The calculated mobility limited by the surface roughness scattering is also higher than the experimental one, and it is a strongly decreasing function of carrier density. Therefore, surface roughness scattering cannot explain the overall behavior of the mobility of our FETs, either. Similarly, the background ionized impurity scattering cannot explain the mobility of our FETs because it leads to a mobility one order of magnitude higher than the experimental one.

The surface impurity scattering with a constant impurity density leads to a slow increase in mobility with carrier density if the distance between the impurities and the two-dimensional hole gas is small (Fig. 3). We calculated the mobility limited by surface charged impurities for different  $n_{\text{imp}}$  by assuming  $d = 0$ . The total mobility calculated with  $n_{\text{imp}} = (1.0-1.5) \times 10^{12} \text{ cm}^{-2}$  agrees reasonably well with the experimental mobility, as shown in Fig. 2. The comparison between the experimental and calculated mobilities thus indicates that the surface impurity scattering is the dominant mechanism that limits the mobility of our FETs.

We assumed  $\Delta=0.3$  nm and  $\Lambda=2$  nm in the calculation of the surface roughness scattering rate. Taking different values of  $\Lambda$  does not considerably influence the carrier density dependence of the mobility for carrier densities lower than  $5 \times 10^{12} \text{ cm}^{-2}$  (Fig. 4(a)). The value of 2 nm for  $\Lambda$  is the same as the one obtained by Li *et al.* This value is also comparable to those used for explaining the mobility in a Si MOSFET<sup>21</sup> and an AlGaIn/GaN heterostructure<sup>22</sup>. The value of  $\Delta$ , in contrast, significantly affects the carrier density dependence of the mo-



bility, as shown in Fig. 4(b). If  $\Delta$  is larger than 1 nm, the mobility decreases rapidly with increasing carrier density. Such a rapid decrease is inconsistent with the experimental results. The experimental mobility can be explained most reasonably with  $\Delta \approx 0.3$  nm. This is within a typical range of surface roughness of polished diamond substrates.

Figure 5 shows the mobilities of heavy, light, and split-off holes as a function of the total hole density. The calculated mobility of the heavy holes is almost the same as the total mobility for each scattering mechanism, indicating the dominant role of heavy holes in carrier transport. This is reasonable because the proportion of the density of heavy holes is the largest. Another feature shown in the figure is that among the mobilities limited by surface impurity scattering, the mobility of the heavy holes is higher than those of the light and split-off holes for a given  $p_{2D}$ . This is mainly because the density and therefore  $k_F$  of the heavy hole subband are the largest. If we plot the impurity-limited mobilities of heavy, light, and split-off holes against each density ( $p^{HH}$ ,  $p^{LH}$ , and  $p^{SO}$ ), the difference between them is small (35% at maximum, which is even smaller than the difference in effective mass  $m_{//}$ ).

Experimentally, the Hall mobility of our FETs was hardly dependent on temperature at  $T > 200$  K (Fig. 4 of Ref. 10), which is consistent with our model with the dominant contribution coming from impurity scattering. At lower temperature, however, the experimental mobility decreases with decreasing temperature (and shows an increase at  $T < 50$  K for high gate voltages). A similar decrease in mobility has been observed in Si MOSFETs<sup>23</sup>. As in the study of Si MOSFETs, we interpret the decrease in mobility to be a result of hole localization caused by potential fluctuations due to the surface charged impurities.

We also examined the mobility of the surface conductivity of the hydrogen-terminated surface exposed to air. The monotonic decrease in mobility with increasing carrier density (Fig. 2) can be explained almost quantitatively by surface impurity scattering with  $n_{imp} = p_{2D}$ , as was reported by Li *et al.*<sup>8</sup>. As an increase in carrier density means an increase in the density of charged impurities, the mobility monotonically decreases with carrier density. In the carrier density range between  $10^{11}$  and  $10^{14}$  cm<sup>-2</sup>, the surface impurity scattering leads to lower mobility than those limited by acoustic phonons and surface roughness; therefore, the surface impurity scattering is dominant. We should note that our calculation used the effective masses for a (111) surface, although Fig. 2 also shows experimental results for (100) surfaces. The difference in calculated mobility between the (100) and (111) surfaces is less

than 40% and is within the variation of the experimental mobilities. We should also note that the contribution of  $N_{\text{depl}}$  is not considered above; more accurately,  $n_{\text{imp}}$  should equal  $p_{2\text{D}} + n_{\text{depl}}$ . We did not find the values of  $n_{\text{depl}}$  of the diamond samples in the literature from which the mobility of the surface conductivity were taken for plotting Fig. 2. The above Schrödinger-Poisson calculations show that  $n_{\text{depl}} = 1.5 \times 10^{12} \text{ cm}^{-2}$  for  $N_{\text{depl}} = 8.8 \times 10^{16} \text{ cm}^{-3}$  (0.5 ppm) and  $n_{\text{depl}} = 4.7 \times 10^{12} \text{ cm}^{-2}$  for  $N_{\text{depl}} = 8.8 \times 10^{17} \text{ cm}^{-3}$  (5 ppm). If  $n_{\text{depl}}$  is taken into account, the calculated mobility decreases with increasing  $n_{\text{depl}}$  especially for low  $p_{2\text{D}}$  (Fig. 6). The dependence of mobility on  $n_{\text{depl}}$  may partly explain why there is a wide distribution of mobilities of surface conductivity in the literature.

The above comparison between the experimental and calculated mobility indicates that the surface impurity scattering is the dominant mechanism that limits the mobility of our FETs. This is consistent with our recent finding that the quantum and transport lifetimes estimated from Shubnikov-de Hass oscillations at low temperatures are nearly the same<sup>24</sup>. The surface charged impurities may be adsorbed when the diamond surface is exposed to air before it is laminated by a flake of h-BN<sup>10</sup>. Most of the heterostructures consisting of graphene and h-BN are also created by stacking the layers with their surfaces exposed to air. The interfaces of the layers can nevertheless be free from adsorbates due to unique self-cleansing effects.<sup>25</sup> However, such self-cleansing effects seem to be ineffective for the interface between the hydrogen-terminated diamond and h-BN. To improve the mobility of the FETs, it would be important to reduce the density of adsorbates, for example, by a vacuum annealing<sup>26</sup>. As shown in Fig. 2, our calculation suggests that decreasing the density of charged impurities to  $\approx 1 \times 10^{11} \text{ cm}^{-2}$  would lead to a mobility above  $1000 \text{ cm}^2 \text{V}^{-1} \text{s}^{-1}$  at room temperature. Surface roughness scattering should also be reduced in the case of carrier densities higher than  $\approx 4 \times 10^{12} \text{ cm}^{-2}$ . For this purpose, it will be effective to use an atomically flat diamond surface prepared by chemical vapor deposition with a low methane concentration on a mesa structure.<sup>27,28</sup>

#### IV. CONCLUSIONS

In conclusion, we calculated the carrier density dependence of the mobility of hydrogen-terminated diamond FETs in consideration of four scattering mechanisms: surface impurity scattering, background ionized impurity scattering, acoustic phonon scattering, and surface

roughness scattering. The calculated mobility agrees with the measured mobility of our diamond FETs with a h-BN gate dielectric if we assume a constant surface impurity density  $n_{\text{imp}} = (1.0 - 1.5) \times 10^{12} \text{ cm}^{-2}$ , average surface roughness  $\Delta$  of 0.3 nm, and correlation length  $\Lambda$  of 2 nm. Decreasing the surface impurity density below  $\approx 1 \times 10^{11} \text{ cm}^{-2}$  will lead to a mobility exceeding  $1000 \text{ cm}^2\text{V}^{-1}\text{s}^{-1}$ . The mobility is significantly higher than that of *p*-type Si MOSFETs and will be useful for developing electronic devices that operate with low loss and high speed.

## ACKNOWLEDGMENTS

We thank T. Teraji and S. Koizumi for their helpful discussions. This study was supported by Grants-in-Aid for Scientific Research (Grants Nos. 25287093, 26630139, 19J12696 and 19H02605) and the “Nanotechnology Platform Project” of MEXT, Japan.

## REFERENCES

- <sup>1</sup>C. J. H. Wort and R. S. Balmer, “Diamond as an electronic material,” *Mater. Today* **11**, 22–28 (2008).
- <sup>2</sup>H. Kawarada, H. Tsuboi, T. Naruo, T. Yamada, D. Xu, A. Daicho, T. Saito, and A. Hiraiwa, “C-H surface diamond field effect transistors for high temperature (400 °C) and high voltage (500 V) operation,” *Appl. Phys. Lett.* **105**, 013510 (2014).
- <sup>3</sup>Y. Kitabayashi, T. Kudo, H. Tsuboi, T. Yamada, D. Xu, M. Shibata, D. Matsumura, Y. Hayashi, M. Syamsul, M. Inaba, A. Hiraiwa, and H. Kawarada, “Normally-off C-H diamond MOSFETs with partial C-O channel achieving 2-kV breakdown voltage,” *IEEE Electron Device Lett.* **38**, 363–366 (2017).
- <sup>4</sup>F. Maier, M. Riedel, B. Mantel, J. Ristein, and L. Ley, “Origin of surface conductivity in diamond,” *Phys. Rev. Lett.* **85**, 3472–3475 (2000).
- <sup>5</sup>M. Kasu, “Diamond field-effect transistors for RF power electronics: Novel NO<sub>2</sub> hole doping and low-temperature deposited Al<sub>2</sub>O<sub>3</sub> passivation,” *Jpn. J. Appl. Phys.* **56**, 01AA01 (2017).
- <sup>6</sup>C. Verona, F. Arciprete, M. Foffi, E. Limiti, M. Marinelli, E. Placidi, G. Prestopino, and G. Verona Rinati, “Influence of surface crystal-orientation on transfer doping of V<sub>2</sub>O<sub>5</sub>/H-

- terminated diamond,” *Appl. Phys. Lett.* **112**, 181602 (2018).
- <sup>7</sup>J. Isberg, J. Hammersberg, E. Johansson, T. Wikstrom, D. J. Twitchen, A. J. Whitehead, S. E. Coe, and G. A. Scarsbrook, “High carrier mobility in single-crystal plasma-deposited diamond,” *Science* **297**, 1670–1672 (2002).
- <sup>8</sup>Y. Li, J.-F. Zhang, G.-P. Liu, Z.-Y. Ren, J.-C. Zhang, and Y. Hao, “Mobility of two-dimensional hole gas in H-terminated diamond,” *physica status solidi (RRL) - Rapid Research Letters* **12**, 1700401 (2018).
- <sup>9</sup>H. Kwarada, T. Yamada, D. Xu, H. Tsuboi, Y. Kitabayashi, D. Matsumura, M. Shibata, T. Kudo, M. Inaba, and A. Hiraiwa, “Durability-enhanced two-dimensional hole gas of C-H diamond surface for complementary power inverter applications,” *Sci Rep* **7**, 42368 (2017).
- <sup>10</sup>Y. Sasama, K. Komatsu, S. Moriyama, M. Imura, T. Teraji, K. Watanabe, T. Taniguchi, T. Uchihashi, and Y. Takahide, “High-mobility diamond field effect transistor with a monocrystalline h-BN gate dielectric,” *APL Materials* **6**, 111105 (2018).
- <sup>11</sup>C. Hamaguchi, *Basic semiconductor physics*, 3rd ed. (Springer, 2017).
- <sup>12</sup>C. Nebel, B. Rezek, and A. Zrenner, “Electronic properties of the 2D-hole accumulation layer on hydrogen terminated diamond,” *Diamond and related materials* **13**, 2031–2036 (2004).
- <sup>13</sup>M. T. Edmonds, C. I. Pakes, and L. Ley, “Self-consistent solution of the schrödinger-poisson equations for hydrogen-terminated diamond,” *Physical Review B* **81**, 085314 (2010).
- <sup>14</sup>R. Winkler, *Spin-orbit Coupling Effects in Two-Dimensional Electron and Hole Systems* (Springer-Verlag Berlin Heidelberg, 2003).
- <sup>15</sup>N. Naka, K. Fukai, Y. Handa, and I. Akimoto, “Direct measurement via cyclotron resonance of the carrier effective masses in pristine diamond,” *Physical Review B* **88**, 035205 (2013).
- <sup>16</sup>J. Cui, J. Ristein, and L. Ley, “Electron affinity of the bare and hydrogen covered single crystal diamond (111) surface,” *Physical Review Letters* **81**, 429 (1998).
- <sup>17</sup>H. B. Michaelson, “The work function of the elements and its periodicity,” *Journal of applied physics* **48**, 4729–4733 (1977).
- <sup>18</sup>J. Pernot, P. N. Volpe, F. Omnès, P. Muret, V. Mortet, K. Haenen, and T. Teraji, “Hall hole mobility in boron-doped homoepitaxial diamond,” *Physical Review B* **81**, 205203

- (2010).
- <sup>19</sup>J. H. Davies, *The physics of low-dimensional semiconductors: an introduction* (Cambridge university press, 1998).
- <sup>20</sup>M. Cardona and N. Christensen, “Deformation potentials of the direct gap of diamond,” *Solid state communications* **58**, 421–424 (1986).
- <sup>21</sup>T. Ando, A. B. Fowler, and F. Stern, “Electronic properties of two-dimensional systems,” *Reviews of Modern Physics* **54**, 437–672 (1982).
- <sup>22</sup>D. Zanato, S. Gokden, N. Balkan, B. K. Ridley, and W. J. Schaff, “The effect of interface-roughness and dislocation scattering on low temperature mobility of 2D electron gas in GaN/AlGaN,” *Semiconductor Science and Technology* **19**, 427–432 (2004).
- <sup>23</sup>F. Fang and A. Fowler, “Transport properties of electrons in inverted silicon surfaces,” *Physical Review* **169**, 619 (1968).
- <sup>24</sup>Y. Sasama, K. Komatsu, S. Moriyama, M. Imura, S. Sugiura, T. Terashima, S. Uji, K. Watanabe, T. Taniguchi, T. Uchihashi, and Y. Takahide, “Quantum oscillations in diamond field-effect transistors with a h-BN gate dielectric,” *Physical Review Materials* **3**, 121601(R) (2019).
- <sup>25</sup>A. V. Kretinin, Y. Cao, J. S. Tu, G. L. Yu, R. Jalil, K. S. Novoselov, S. J. Haigh, A. Gholinia, A. Mishchenko, M. Lozada, T. Georgiou, C. R. Woods, F. Withers, P. Blake, G. Eda, A. Wirsig, C. Hucho, K. Watanabe, T. Taniguchi, A. K. Geim, and R. V. Gorbachev, “Electronic properties of graphene encapsulated with different two-dimensional atomic crystals,” *Nano Lett.* **14**, 3270–3276 (2014).
- <sup>26</sup>M. Inaba, H. Kawarada, and Y. Ohno, “Electrical property measurement of two-dimensional hole-gas layer on hydrogen-terminated diamond surface in vacuum-gap-gate structure,” *Applied Physics Letters* **114**, 253504 (2019).
- <sup>27</sup>N. Tokuda, H. Umezawa, S.-G. Ri, M. Ogura, K. Yamabe, H. Okushi, and S. Yamasaki, “Atomically flat diamond (111) surface formation by homoepitaxial lateral growth,” *Diamond and Related Materials* **17**, 1051–1054 (2008).
- <sup>28</sup>Y. Takahide, H. Okazaki, K. Deguchi, S. Uji, H. Takeya, Y. Takano, H. Tsuboi, and H. Kawarada, “Quantum oscillations of the two-dimensional hole gas at atomically flat diamond surfaces,” *Phys. Rev. B* **89**, 235304 (2014).

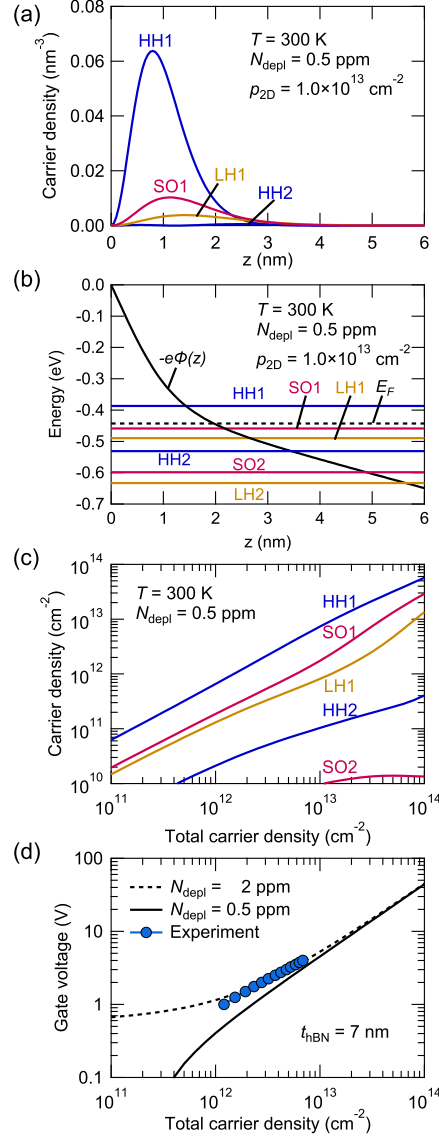


FIG. 1. (a) Calculated density profile of the lowest subbands of heavy- (HH), light- (LH), and split-off (SO) holes and the second subband of heavy holes (HH2) for the total carrier density of  $1.0 \times 10^{13} \text{ cm}^{-2}$  at  $T = 300 \text{ K}$ .  $z$  is the depth from the diamond surface.  $N_{\text{depl}}$  is assumed to be 0.5 ppm. (b) Calculated potential energy, Fermi level, and maximum of the first and second subbands of heavy, light, and split-off holes as a function of  $z$ . (c) Calculated population of heavy holes, light holes, and split-off holes as a function of total carrier density at  $T = 300 \text{ K}$ . (d) Calculated gate voltage vs. total carrier density for  $t_{\text{hBN}} = 7 \text{ nm}$  thick gate dielectric.  $N_{\text{D}} = 0.5 \text{ ppm}$  and  $N_{\text{A}} = 5 \text{ ppb}$  for the solid line and  $N_{\text{D}} = 2 \text{ ppm}$  and  $N_{\text{A}} = 5 \text{ ppb}$  for the dashed line.  $n_{\text{imp}} = 1.5 \times 10^{12} \text{ cm}^{-2}$  for both curves. Experimental results of our h-BN/diamond FET (Fig. 2(c) of Ref. 10) are also shown.

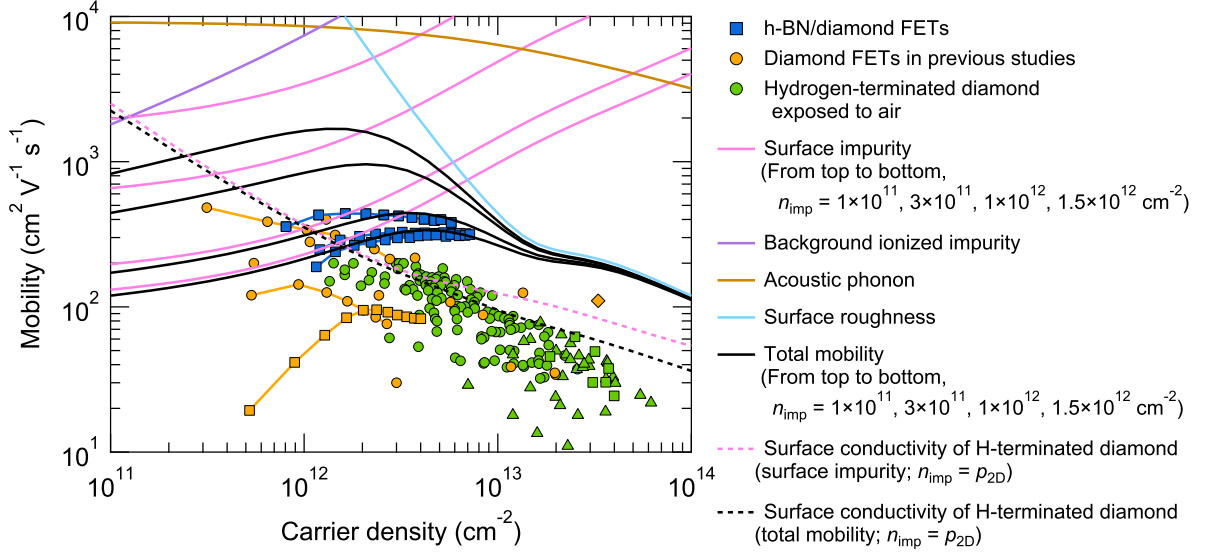


FIG. 2. Carrier density dependence of mobility. Solid lines show calculated results for hydrogen-terminated diamond FETs. Dashed lines show calculated results for the surface conductivity of hydrogen-terminated diamond exposed to air. The figure also shows experimental results<sup>10</sup> for our h-BN/diamond FETs, other groups' diamond FETs and surface conductivities of hydrogen-terminated diamond exposed to air. Squares, circles, and triangles represent (111), (100), and (110) diamond surfaces, respectively. The rhombus represents polycrystalline diamond.

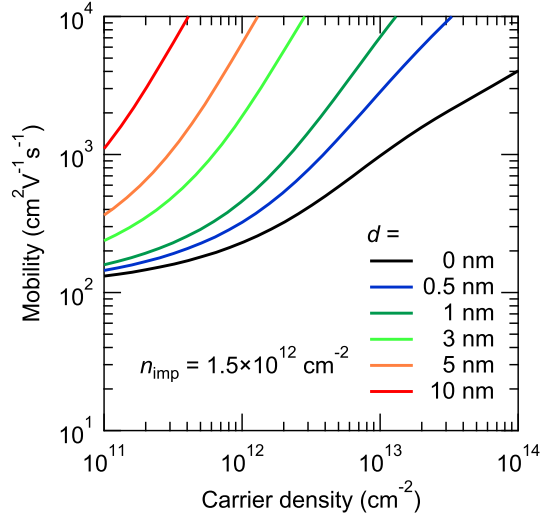


FIG. 3. Calculated carrier density dependence of mobility limited by surface impurity scattering. The density of surface charged impurities  $n_{\text{imp}}$  is  $1.5 \times 10^{12} \text{ cm}^{-2}$ .  $d$  is the distance between the charged impurities and the two-dimensional hole gas.

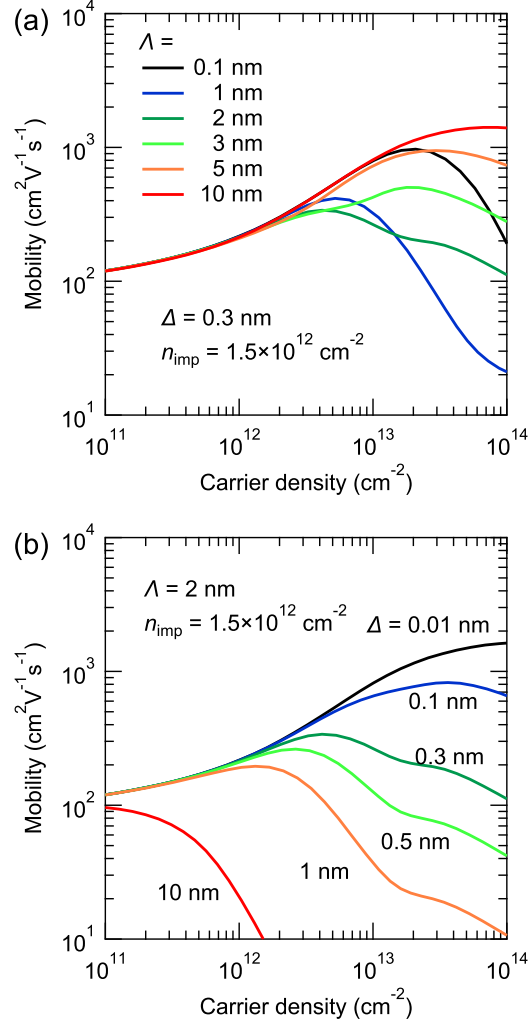


FIG. 4. (a) Calculated carrier density dependence of mobility for different values of  $\Lambda$ .  $\Delta$  is 0.3 nm, and  $n_{\text{imp}}$  is  $1.5 \times 10^{12}$  cm<sup>-2</sup>. (b) Calculated carrier density dependence of mobility for different values of  $\Delta$ .  $\Lambda$  is 2 nm, and  $n_{\text{imp}}$  is  $1.5 \times 10^{12}$  cm<sup>-2</sup>.



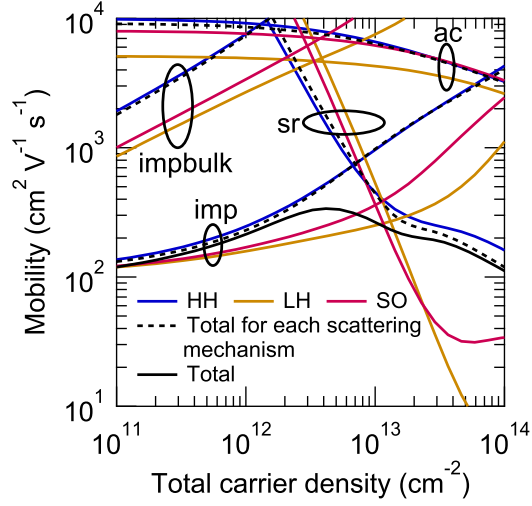


FIG. 5. Calculated mobilities for heavy, light, and split-off holes as a function of the total hole density. The black solid line represents the total mobility. The black dashed lines represent the total mobility for each scattering mechanism. imp, impbulk, ac, and sr indicate surface impurity, background ionized impurity, acoustic phonon, and surface roughness scattering, respectively.

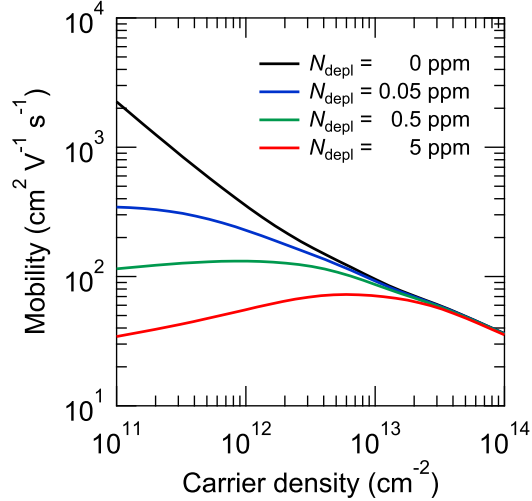


FIG. 6. Calculated carrier density dependence of mobility for the surface conductivity of hydrogen-terminated diamond for different values of  $N_D = 0, 0.05, 0.5$  and  $5$  ppm with  $N_A/N_D$  kept to be  $0.01$ . The calculation was performed assuming  $n_{\text{imp}} = p_{2D} + n_{\text{depl}}$ .